Multi-stage risk-based assessment for wind energy accommodation capability: a robust and non-anticipative method

Houbo Xiong[a], Yue Zhou[b,*], Chuangxin Guo[a,*], Yi Ding[a], Fengji Luo[c]

[a]*College of Electrical Engineering, Zhejiang University, Hangzhou 310027, China*
[b]*School of Engineering, Cardiff University, Cardiff CF24 3AA, UK*
[c]*School of Civil Engineering, University of Sydney, Sydney, NSW 2006, Australia*

HIGHLIGHTS

- A novel assessment method for WAC is proposed based on the multi-stage robust optimization.
- Tractable risk evaluation method is integrated in the multi-stage framework.
- Adaptive techniques are designed for FRDDP method to accelerate the optimal solution.
- The proposed method achieves both non-anticipative and robust assessment decisions.

ARTICLEINFO

Keywords:
Uncertainty
Wind energy
Accomoation capability assessment
Non-anticipativity
Multi-stage robust optimization
Dynamic programming

ABSTRACT

The volatility and uncertainty of wind energy has brought great challenges to its accommodation in electric power systems. To determine a wind power trading strategy in the real-time power market, the accurate assessment of wind energy accommodation capability (WAC) is of great significance. However, most current studies investigate the wind energy accommodation potential from the perspective of dispatch, but rarely provide quantitative assessment results. Additionally, the non-anticipativity of decisions has not been considered in the assessment yet. This paper proposes a novel quantitative assessment method for WAC based on the multi-stage robust optimization (RO), which addresses the anticipativity issues in the traditional two-stage method while maintaining the decision-making process' robustness. In the assessment method, the operational risk is integrated via a tractable scheme to obtain dynamic admissible WAC boundaries. To obtain the optimal solution of the proposed multi-stage RO problem, a fast robust dual dynamic programming (FRDDP) algorithm is employed, where the adaptive techniques are developed to accelerate the computation. Numerical studies on the modified IEEE 14-Bus system and a real-world system in Zhejiang Province of China validate the effectiveness of the proposed assessment model and adaptive acceleration techniques. The simulation results demonstrate the presented method brings a 18.87% reduction in operational cost, and reduces 29.34% curtailment of wind energy. Compared with the original FRDDP, the adaptive technique significantly reduces the computational consumption by 73.34% on the real-world test system.

1. Introduction

The wind energy installed capacity has rapidly expanded to mitigate global warming caused by excessive fossil fuel consumption since it can provide electricity with zero carbon emissions [1], [2]. However, the endogenous variability and uncertainty characteristics make wind energy difficult to be accommodated in power systems [3]. In some real-time power markets, power system operators need to purchase electricity from wind farms [4]. When the actual available wind energy in the market cannot support the demand, operators will make additional emergency regulations, such as running fast-acting units to recover the operation feasibility [5]. Thus, the wind power accommodation capability (WAC) assessment results are necessary to give the range of wind power that can be purchased from the market, and provide the boundary conditions of wind power output for

Nomenclature

Abbreviations

WAC	Wind energy accommodation capability
RO	Robust optimization
FRDDP	Fast robust dual dynamic programming
SO	Stochastic optimization
SDDP	Stochastic dual dynamic programming
RDDP	Robust dual dynamic programming
RIA	Relaxed inner approximation
UC	Unit Commitment
ED	Economic dispatch
ESS	Energy storage systems

ℓ_t^v	The penalty coefficient of slack variables
$\overline{\theta}$, $\underline{\theta}$	Upper/lower bound of phase angles
$\overline{F}_{hk}$, $\underline{F}_{hk}$	Upper/lower capacity limits of transmission line hk
ρ	Penalty factor of ℓ_t^v in RIA
C_e	Total capacity of ESS e
$\wp_s$	The objective value of upper approximation problem in s
c_q^e, c_q^d	Coefficients of operational risk
M	Penalty factors of imbalanced power
$\omega_{q,t,\gamma}^+$, $\vartheta_{q,t,\gamma}^+$	Intermediate parameters of piecewise linearization method
$\overline{P}_g$, $\underline{P}_g$	Upper/lower generation limitation of unit g

WCR	Wind curtailment risk	$I_{g,t}$	Pre-defined UC plan in unit g, period t
LSR	Load shedding risk	R_g^+, R_g^-	Ramp up/down rate limit of unit g
SOC	State of charge	$\overline{A}_q$	Upper limit of available wind power in farm q
MI14B	Modified IEEE 14-Bus	$\overline{Soc}_e$, $\underline{Soc}_e$	Upper/lower limits state of charge in ESS e
FEG	Fast-starting emergency generator	$L_{d,t}$	Load demand of node d at period t
MC	Monte Carlo method	*Variables*	
Indices and Sets		$Risk_t^{+(-)}$	Measurement for WCR and LSR
$q \in \mathcal{W}$	Index of wind farms	$Aw_{q,t}^{+(-)}$	Upper/lower bound of WAC range in wind farm q at period t
$g \in \mathcal{G}$	Index of thermal units	$P_{g,t}$	Output of unit g at period t
$e \in \mathfrak{C}$	Index of ESS	$Aw_{q,t}$	Available wind power in wind farm q at period t
$h \in \mathcal{B}$	Index of power buses	$\xi_{q,t}^{+(-)}$	Uncertainty indicator variables in wind farm q at period t
$hk \in \mathcal{L}$	Index of transmission lines	$Soc_{e,t}$	State of charge of ESS e at period t
$s \in \Lambda_t$	Index of valid iterations/sampling points at stage t	$Pe_{e,t}$	Charging/discharging power of ESS e at period t
$d \in \mathcal{D}$	Index of demands	$Pw_{q,t}$	Consumed wind power in wind farm q at period t
$\mathcal{L}f_h / \mathcal{L}t_h$	Sets of lines come from/to node h	$\theta_{h,t}$	Phase angle of node h at period t
Ω	Feasible set of admissible WAC decision	$F_{hk,t}$	Power flow at line hk at period t
Φ	Feasible set of dispatch decision	$\delta_{h,t}^{+(-)}$	Slack variables in Bus h for power flow at period t
Ξ	Uncertainty set of wind power	$\Delta_t^{+(-)}$	Slack variables for characterizing sampling points at period t
$\mathbb{R}^n$	Set of n-dimensional real variables	λ_s	The coefficients of the convex combination in iteration s
Parameters			
ς	Quantity measurement of wind generation		
γ	Ordinal number of the piecewise linearization method		
$a_{q,t,\gamma}^+$, $b_{q,t,\gamma}^+$	Constant coefficients of operational risk		

the secure and economic operation of power systems [5], [6]. An effective WAC assessment method needs to meet the following requirements:

- Properly modeling the uncertainty of wind generation, and
- Obtaining quantitative assessment results.

To cope with the uncertainties of wind power, the two-stage stochastic optimization (SO) methodology was presented in [7]-[10]. Nevertheless, the SO approach is hard to be applied in practice due to the computational intractability and the requirement of accurate distribution of the random variables [11]. An alternative approach is the robust optimization (RO) method, which mitigates computational burden via using the "max-min" operator to screen out the worst-case scenario [12]. Benefiting from this, the two-stage RO is frequently utilized in modeling the operation of variable renewable systems [13]-[15], and has been applied in providing a robust WAC assessment [6].

Despite their demonstrated effectiveness, the state-of-the-art two-stage SO and RO approaches violate the non-anticipativity of decisions under the evolution of uncertain wind energy [16], [17]. Specifically, the second stage decisions of two-stage scheme are made with the full knowledge of all the uncertain parameters in the future, while in the real-world process, the system operators' decisions only depend on the uncertainties realized up to the current period [18]. Consequently, the two-stage scheme overestimates the adjustment capacity of power systems to accommodate wind energy [19].

To enforce the non-anticipativity of decisions, temporal decomposition is employed to extend the two-stage SO and RO into a multi-stage problem. In the field of SO, the multi-stage version has recently attracted a lot of interests, and performs well in hydropower scheduling [17], economic dispatch [20], microgrid operation [18], and long-time planning [21]. Besides, a sequential solution method, referred to stochastic dual dynamic programming (SDDP) [20], can provide the global optimal solution to the multi-stage SO. Compared to SO, the research in RO is lagging in the multi-stage field, since it is challenging to find a tractable way for tackling the nested "max-min" operators [22]. The conventional solution method is to use the affine rules [23] to map the unit output to a linear function of the actual wind power [24]. To improve the optimality, the piecewise affine rules [25]-[26] and the polynomial affine rules [27] are proposed. Although the different affine rules seem to provide an executable way to handle the multi-stage RO model, it should be emphasized that they are essentially conservative approximation ways, which oversimplifies the origin formulation and reduces the quality of solution. Recently, a mathematically

Table 1. Comparative features of relevant studies pertaining to WAC

Reference	Quantitative assessment results	Non-anticipative decisions	Risk-based evaluation	Global optimality	Acceleration of solution algorithm
[16], [22], [25]	×	✓	×	×	×
[19], [29], [30]	×	✓	×	✓	×
[34]	✓	×	×	✓	×
[5], [6], [35], [36]	✓	×	✓	✓	×
This work	✓	✓	✓	✓	✓

strict robust dual dynamic programming (RDDP) method is proposed to achieve the global solution of multi-stage RO model [28], which is a robust counterpart of SDDP. However, since the method used in the upper approximation of RDDP has exponentially increasing time complexity, it is not suitable for solving the real-time dispatch problem even with more than ten units [28], [29]. In [30], the column and constraint generation

algorithm is integrated to RDDP for improving the tractability. In our previous work, a fast RDDP (FRDDP) method through relaxed inner approximation (RIA) is proposed [31]. Through testing, FRDDP significantly improves the solution speed of traditional RDDP. In [32], the RIA and outer approximation are simultaneous utilized to construct an upper bound for the non-convex value functions under the RDDP based framework. However, the latest studies [29]-[32] of modeling the uncertainties of wind energy focus on the power dispatch, whose application in tackling the WAC assessment problem is still a gap.

Referring to the studies aforementioned above, most of them investigate the wind energy accommodation potential of power systems from the perspective of dispatch, but no quantitative WAC assessment results are given [19], [33]. In [34], a do-not-exceed limitation interval of wind energy is proposed to achieve the WAC assessment of power grids. However, this method can only provide a static WAC assessment result since it is derived under a pre-defined box uncertainty set, which may not be optimal under different real-time dispatch strategies. Ref. [5] and Ref. [35] minimize the operational risk to measure the admissible wind energy, which can obtain a dynamic WAC assessment outcome being fit for different economic dispatch (ED) strategies. Furthermore, Ref. [36] considers the information of wind generation forecast errors in the risk measurement to achieve a more accurate WAC assessment. In [6], the operational risk is divided into the wind curtailment and load shedding risk, where a tractable linearization method is also presented. However, the existing studies that can provide a quantitative WAC assessment [5]-[6], [35]-[36], are formulated by the two-stage RO approach, which violates the non-anticipativity of decisions under the uncertain wind energy. Thus, the WAC assessment outcomes from them will lose accuracy.

The challenges existed in the literature in terms of presenting an effective WAC assessment method can be summarized as follows:

(1) Most research investigates the WAC potential from the perspective of dispatch, but rarely provides quantitative assessment results.

(2) Although a few attempts have been made on the quantitative assessment of WAC, they formulate the uncertainty of wind energy based on the two-stage scheme, which violates the non-anticipativity of assessment decisions.

(3) A WAC assessment method that can provide dynamic admissible boundaries and properly evaluate systems' operational risk is still lacking.

To address these challenges, this paper proposes an innovative WAC assessment method, which can provide quantitative assessment outcomes of WAC for directing the development of real-time trading strategies for power systems that need to purchase electricity from wind farms. The proposed method enforces the non-anticipativity of assessment decisions and designs a risk-based measurement technique to serve a dynamic assessment result. The main contributions of this work are as follows, compared with the existing studies in Table 1.

(1) The proposed method can provide a quantitative range of WAC to power system operators, which can be served as the real-time wind power purchasing guidance for power systems.

(2) Based on the multi-stage RO model, the proposed method enforces the non-anticipativity and preserves the robustness of decision-making, which improves the accuracy of assessment results compared to the existing studies.

(3) The multi-stage scheme is presented with a tractable strategy for evaluating operational risk, enabling the proposed WAC assessment method to obtain dynamic acceptable boundaries in accordance with the operation risk of the systems.

(4) A novel FRDDP algorithm is employed as the global optimal solution methodology. For accelerating computation, we develop two adaptive techniques.

The remainder of this paper is organized as follows. Section 2 introduces the concept of WAC assessment in power systems. Section 3 describes the mathematical formulation of the proposed WAC assessment model. Section 4 illustrates the FRDDP solution methodology and the developed adaptive acceleration techniques. In Section 5, the proposed assessment model and solution methodology are validated on a modified IEEE 14-Bus system and a real-world system in Zhejiang province of China. Section 6 concludes this paper.

2. Concept of WAC assessment in power systems

In recent decades, more and more individual wind power operators have participated in power markets [37]. This study focuses on the power systems that need to purchase wind energy from wind power operators in real-time power market [38], the mechanism of which is shown by Fig. 1. During the day-ahead stage, under the pre-determined unit commitment (UC), power system operators aggregate the forecast wind power information, the adjusting capacity of dispatchable units and energy storage systems (ESS), and the gird parameters to assess WAC. The schematic diagram is shown in Fig. 2. In the intra-day stage, the obtained WAC range is utilized to evaluate the impact of real measured wind power for power systems and makes corresponding dispatch and trading plan.

As shown in Fig.2, if the real measured wind power located in the WAC range (i.e., admissible region), power system operators can purchase the entire volume of wind power, since arbitrary realization of wind generation within the range can be fully admitted without breaking the operational feasibility. When the real measured wind power exceeds the upper bound of WAC, the maximum quantity that can be purchased by the operators is restricted by the upper admissible level, since the adjusting capacity of dispatchable units and ESS cannot support consuming the abundant wind generation, which leads to the power imbalance. Once the real measured wind power is smaller than the lower bound of WAC range, fast-starting emergency units that are not contained in the day-ahead UC plan, are started up to preserve normal demand.

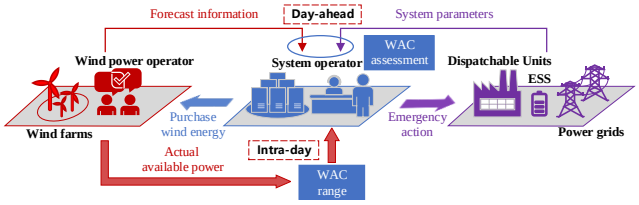

Fig. 1. The mechanism representation of WAC assessment in energy scheduling and trading

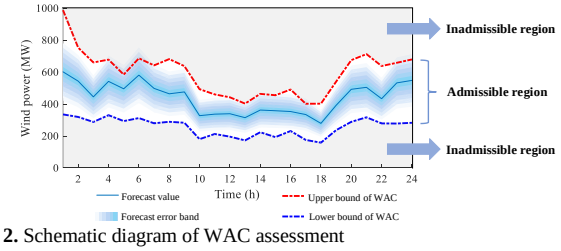

Fig. 2. Schematic diagram of WAC assessment

3. Mathematic formulation of proposed WAC assessment method

3.1. Tractable operational risk evaluation model

The operational risk is defined referring to [5] and [35], which is the expectation of wind curtailment risk (WCR) and the load shedding risk (LSR) when the wind power exceeds the system's WAC range. It is usually established based on the probability distribution function of wind power, which is obtained by the historical prediction error data.

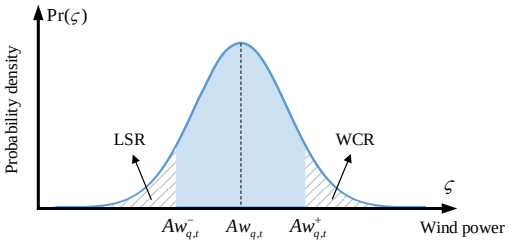

Fig. 3. Probability density function of wind power and operational risk

The relationship between WAC and operational risk can be seen in Fig. 3, where $Aw_{q,t}$ represents the day-ahead forecast wind power. Arising from the forecast error, when the intra-day actual wind power is larger than the upper bound of WAC range, $Aw^+_{q,t}$, it will result in WCR. Conversely, when the actual wind power is smaller than $Aw^-_{q,t}$, it will cause LSR, which needs emergency regulations to restore systems' operational feasibility, as described in Section 2. According to the definition of operational risk, WCR and LSR can be calculated by (1) and (2), respectively:

$$Risk^+_{q,t} = c^u_q \int_{Aw^+_{q,t} \le \varsigma \le \overline{A}_q} (\varsigma - Aw^+_{q,t}) \Pr(\varsigma) d(\varsigma) \tag{1}$$

$$Risk^-_{q,t} = c^d_q \int_{0 \le \varsigma \le Aw^-_{q,t}} (Aw^-_{q,t} - \varsigma) \Pr(\varsigma) d(\varsigma) \tag{2}$$

where, ς is the quantity of wind generation, and $\Pr(\varsigma)$ stands for its probability.

Since the defined formula of operational risk (1) and (2) contain complex integral terms, a piece-wise linear method is introduced for reformulating it into a tractable model. Since the operational risk is always convex for different kinds of probability density functions [39], this tractable operational risk model is valid for any probability density functions of wind energy. Taking WCR as an example, the first step is to relax (1) to inequality (3):

$$Risk^+_{q,t} \ge c^u_q \int_{Aw^+_{q,t} \le \varsigma \le \overline{A}_q} (\varsigma - Aw^+_{q,t}) \Pr(\varsigma) d(\varsigma) \tag{3}$$

Since the operation risk is minimized in the objective function, (3) will take an equal sign after optimization, which means formula (1) and (3) are equivalent. Furthermore, (3) is piecewise linearized as (4):

$$Risk^+_{q,t} \ge a^+_{q,t,\gamma} Aw^+_{q,t} + b^+_{q,t,\gamma}, \ \forall q \in \mathcal{W}, t, \gamma \tag{4}$$

where, γ is ordinal number of the piecewise linearization method. $a^+_{q,t,\gamma}$ and $b^+_{q,t,\gamma}$ are the constant coefficients, which can be calculated by (5)-(8):

$$\vartheta^+_{q,t,\gamma} = (\gamma - 1)\Delta\gamma \tag{5}$$

$$\omega^+_{q,t,\gamma} = c^u_q \int_{\vartheta^+_{q,t,\gamma} \le \kappa \le \overline{A}_q} (\kappa - \vartheta^+_{q,t,\gamma}) \Pr(\kappa) d(\kappa) \tag{6}$$

$$a^+_{q,t,\gamma} = (\omega^+_{q,t,\gamma+1} - \omega^+_{q,t,\gamma}) / (\vartheta^+_{q,t,\gamma+1} - \vartheta^+_{q,t,\gamma}) \tag{7}$$

$$b^+_{q,t,\gamma} = -\vartheta^+_{q,t,\gamma} (\omega^+_{q,t,\gamma+1} - \omega^+_{q,t,\gamma}) / (\vartheta^+_{q,t,\gamma+1} - \vartheta^+_{q,t,\gamma}) + \omega^+_{q,t,\gamma} \tag{8}$$

Similarly, the LSR can be reformulated by the tractable formula:

$$Risk^-_{q,t} \ge a^-_{q,t,\gamma} Aw^-_{q,t} + b^-_{q,t,\gamma}, \ \forall q \in \mathcal{W}, t, \gamma \tag{9}$$

3.2. System secure operation constraints

The generation of dispatchable units are limited by constraints (10)-(12), which include the upper and lower generation limits and ramping restrictions. The start-up or shut-down state of units are fixed by the day-ahead determined UC plan $I_{g,t}$.

$$\underline{P}_g I_{g,t} \le P_{g,t} \le \overline{P}_g I_{g,t}, \forall g \in \mathcal{G}, t \tag{10}$$

$$P_{g,t} - P_{g,t-1} \le I_{g,t-1} R^+_g + \left(1 - I_{g,t-1}\right) \overline{P}_g, \forall g \in \mathcal{G}, t \tag{11}$$

$$P_{g,t-1} - P_{g,t} \le I_{g,t} R^-_g + \left(1 - I_{g,t}\right) \overline{P}_g, \forall g \in \mathcal{G}, t \tag{12}$$

The output of wind generation is characterized by (13)-(15). Among them, (13) regulates the relationship between the forecast available wind power and WAC range. (14) restricts that the consumed wind power cannot exceeds the real measured wind power, which fluctuates within the uncertainty set. (15) defines the boundary of uncertainty sets of real measured wind power, where $\xi^+_{q,t}$, $\xi^-_{q,t}$ are binary variables.

$$0 \le Aw^-_{q,t} \le Aw_{q,t} \le Aw^+_{q,t} \le \overline{A}_q, \forall q \in \mathcal{W}, t \tag{13}$$

$$0 \le Pw_{q,t} \le Aw_{q,t} + \xi^+_{q,t}(Aw^+_{q,t} - Aw_{q,t}) - \xi^-_{q,t}(Aw_{q,t} - Aw^-_{q,t}), \forall q \in \mathcal{W}, t \tag{14}$$

$$\xi^-_{q,t} + \xi^+_{q,t} \le 1, \forall q \in \mathcal{W}, t \tag{15}$$

The charging and discharging states of ESS are often represented by two separate integer variables to consider the different charging and discharging efficiencies, which will cause intractable problems in large-scale multi-stage SO or RO problems [20]. In our previous work [19], [31], a tractable ESS model is proposed in a multi-stage RO problem, whose effectiveness also has been mathematically proved. This study also adopts this linear ESS model, which is specifically shown as follows:

$$Soc_{e,t-1} - Pe_{e,t} \eta^c_e / C_e \le \overline{Soc}_e, \forall e \in \mathfrak{C}, t \tag{16}$$

$$Soc_{e,t-1} - Pe_{e,t} / (\eta^d_e C_e) \ge \underline{Soc}_e, \forall e \in \mathfrak{C}, t \tag{17}$$

$$Soc_{e,t} = Soc_{e,t-1} - Pe_{e,t} / C_e, \forall e \in \mathfrak{C}, t \tag{18}$$

where, the positivity or negativity of $Pe_{e,t}$ represents the charging or discharging of ESS. The state of charge (SOC) of ESS are limited by (16) and (17). Eq. (18) is an approximated computation to model the transformation of SOC for ESS, which ignores the charging and discharging efficiency parameters of ESS.

Then, the deviation for SOC caused by the ignorance of efficiency is refined by correction function (19). Note that (19) does not serve as a constraint and is calculated in the interval of each adjacent stage of multi-stage RO problem, so the max/min operators will not affect the model's linearity [19].

$$Soc_{e,t} = Soc_{e,t-1} - \max\left\{Pe_{e,t}, 0\right\} / (\eta^d_e C_e) - \eta^c_e \min\left\{Pe_{e,t}, 0\right\} / C_e, \forall e \in \mathfrak{C}, t \tag{19}$$

The DC power flow [29] is utilized to model the power balance of the whole network. Constraints (20)-(21) characterizes the relationship of phase angle difference and power flow between the connected nodes. (22) restricts the power flow in each transmission line within the capacity limitation. Constraint (23) stipulates the nodal power balance.

$$\left(\theta_{h,t} - \theta_{k,t}\right) / x_{hk} = F_{hk,t}, \forall hk \in \mathcal{L}f_h \cup \mathcal{L}t_h, t \tag{20}$$

$$\underline{\theta} \le \theta_{h,t} \le \overline{\theta}, \forall h \in \mathcal{B}, t \tag{21}$$

$$-\underline{F}_{hk} \le F_{hk,t} \le \overline{F}_{hk}, \forall hk \in \mathcal{L}, t \tag{22}$$

$$\begin{aligned} &\sum_{g \in \mathcal{G}_h} P_{g,t} + \sum_{e \in \mathfrak{C}_h} Pe_{e,t} + \sum_{q \in \mathcal{W}_h} Pw_{q,t} - \sum_{hk \in \mathcal{L}f_h} F_{hk,t} \\ &+ \sum_{hk \in \mathcal{L}t_h} F_{hk,t} = \sum_{d \in \mathcal{D}_h} L_{d,t} + \delta^+_{h,t} - \delta^-_{h,t}, \forall h \in \mathcal{B}, t \end{aligned} \tag{23}$$

3.3. Overall multi-stage RO based WAC assessment problem

By minimizing the anticipated operational risk brought on by the inadmissible wind energy, the WAC range can be obtained, which needs to consider the worst-case scenario to guarantee the operational feasibility. This renders a multi-layer optimization problem as follows:

$$\min_{\boldsymbol{w}=[\boldsymbol{w}_1,\boldsymbol{w}_2,...,\boldsymbol{w}_T]} \sum_{t\in[1:T]}\sum_{q\in\mathcal{W}} Risk^{+}_{q,t} + Risk^{-}_{q,t}$$
$$s.t.\ \ (4),\ (9),\ (13) \tag{24}$$
$$\text{For } \forall t:\ \boldsymbol{w}_t \in \left\{ \begin{array}{l} \max\limits_{\boldsymbol{\xi}_t} \min\limits_{\boldsymbol{p}_t} \sum\limits_{t\in[1:T]}\sum\limits_{h\in\mathcal{B}} M(\delta^{+}_{h,t} - \delta^{-}_{h,t}) \\ s.t.\ \ \delta^{+}_{h,t} \ge 0,\ \delta^{-}_{h,t} \ge 0, \\ (10)-(12),\ (14)\text{-}(15),\ (16)\text{-}(18),\ (20)\text{-}(23) \end{array} \middle| \ \forall t \right\}$$

where:

$$\boldsymbol{w}_t = \{Aw^{+}_{q,t}, Aw^{-}_{q,t} \mid q\in\mathcal{W}\}, \boldsymbol{\xi}_t = \{\xi^{+}_{q,t}, \xi^{-}_{q,t} \mid q\in\mathcal{W}\}, \boldsymbol{p}_t = \{P_{g,t}, Soc_{e,t},$$
$$Pe_{e,t}, Pw_{q,t}, \theta_{h,t}, F_{hk,t}, \delta^{+}_{h,t}, \delta^{-}_{h,t} \mid g\in\mathcal{G}, e\in\mathfrak{C}, q\in\mathcal{W}, hk\in\mathcal{L}, h\in\mathcal{B}\}$$

In problem (24), the out-layer "min" problem ensures the optimality of WAC boundaries in terms of system operational risk. The inner-layer "max-min" problems are nested in sequence for $t \in [1{:}T]$, which guarantees within the admissible WAC decision $\boldsymbol{w}_t$, arbitrary wind generation realizations will not cause power imbalance.

For the brevity of statements, the multi-stage RO based WAC assessment problem can be recast in the compact problem (25).

$$\min_{\boldsymbol{w}\in\Omega}\left\{\boldsymbol{c}^{\top}\boldsymbol{w} + \max_{\boldsymbol{\xi}_1\in\Xi_1} \min_{\boldsymbol{p}_1\in\Phi_1(\boldsymbol{w}_1,\boldsymbol{\xi}_1,\boldsymbol{p}_0)} \left\{\boldsymbol{m}_1^{\top}\boldsymbol{p}_1 + \cdots + \max_{\boldsymbol{\xi}_T\in\Xi_T} \min_{\boldsymbol{p}_T\in\Phi_T(\boldsymbol{w}_T,\boldsymbol{\xi}_T,\boldsymbol{p}_{T-1})} \boldsymbol{m}_T^{\top}\boldsymbol{p}_T\right\}\right\}$$
$$\begin{aligned} s.t.\quad & \boldsymbol{A}\boldsymbol{w} \le \boldsymbol{h} \quad \boldsymbol{w} = [\boldsymbol{w}_1, \boldsymbol{w}_2, ..., \boldsymbol{w}_T] \in \mathbb{R}^{m\times T} \\ & \boldsymbol{B}_1\boldsymbol{p}_1(\boldsymbol{\xi}_1) + \boldsymbol{E}_1\boldsymbol{w}_1 \le \boldsymbol{F}_1\boldsymbol{\xi}_1 \\ & \boldsymbol{D}_t\boldsymbol{p}_{t-1}(\boldsymbol{\xi}_{t-1}) + \boldsymbol{B}_t\boldsymbol{p}_t(\boldsymbol{\xi}_t) + \boldsymbol{E}_t\boldsymbol{w}_t \le \boldsymbol{F}_t\boldsymbol{\xi}_t \quad \forall t = 2,...,T \\ & \boldsymbol{p}_t(\boldsymbol{\xi}_t) \in \mathbb{R}^n, \boldsymbol{\xi}_t \in \Xi_t, \forall t = 1,...,T \end{aligned} \tag{25}$$

where, the "max-min" operators screen out the worst-case wind generation scenario to determine a WAC assessment result that is secure enough for system operational feasibility. Compared to the two-stage RO based method, the "max-min" operators are sequentially expanded to multi-stage, which follow the non-anticipative evolution of uncertainty realizations, discussed in [19] in more detail.

To decouple $\boldsymbol{p}_t$ and $\boldsymbol{\xi}_t$ from the complex affine relationship $\boldsymbol{p}_t(\boldsymbol{\xi}_t)$, problem (25) can be equivalently transformed to the L-shaped nested form, according to the dynamic programming methodology [19].

$$\begin{aligned} Q_P = \min\ & \boldsymbol{c}^{\top}\boldsymbol{w} + \mathcal{Q}_1(\boldsymbol{w}) \\ s.t.\ & \boldsymbol{A}\boldsymbol{w} \le \boldsymbol{h} \\ & \boldsymbol{w} = [\boldsymbol{w}_1, \boldsymbol{w}_2, ..., \boldsymbol{w}_T] \in \mathbb{R}^{m\times T} \end{aligned} \tag{26}$$

where, $\mathcal{Q}_1(\boldsymbol{w})$ is the worst-case cost-to-go function of pre-stage problem Q_P, which measures the total operational risk of WAC assessment decision $\boldsymbol{w}$ under for whole intra-day system operation. The $\mathcal{Q}_1(\boldsymbol{w})$ can be calculated by: $\mathcal{Q}_1(\boldsymbol{w}) = \max\{Q_1(\boldsymbol{w}; \boldsymbol{\xi}_1): \boldsymbol{\xi}_1 \in \Xi_1\}$.

Following the paradigm of dynamic programming, $\boldsymbol{w}$ is sent to the system operation problems (Q_1 to Q_T) as a state-variable, which begins with the 1-stage problem (27).

$$\begin{aligned} Q_1(\boldsymbol{w};\boldsymbol{\xi}_1) = \min\ & \boldsymbol{m}_1^{\top}\boldsymbol{p}_1 + \mathcal{Q}_2(\boldsymbol{\omega}_1, \boldsymbol{p}_1) \\ s.t.\ & \boldsymbol{\omega}_1 = \boldsymbol{w} \\ & \boldsymbol{B}_1\boldsymbol{p}_1 + \boldsymbol{E}_1\boldsymbol{\omega}_1\boldsymbol{e}_1 \le \boldsymbol{F}_1\boldsymbol{\xi}_1 \\ & \boldsymbol{p}_1 \in \mathbb{R}^n,\ \boldsymbol{\omega}_1 \in \mathbb{R}^{m\times T} \end{aligned} \tag{27}$$

where, $\boldsymbol{e}_1$ is a selection matrix which selects the $\boldsymbol{w}_1$ from $\boldsymbol{w}$.

The cost-to-go functions $\mathcal{Q}_t(\boldsymbol{\omega}_{t-1}, \boldsymbol{p}_{t-1})$ of system operation problems, where $t \ge 2$, encode the future power imbalance penalty of operation strategies and assessment decisions $(\boldsymbol{\omega}_{t-1}, \boldsymbol{p}_{t-1})$ in the worst case. It can be calculated by:

$$\mathcal{Q}_t(\boldsymbol{\omega}_{t-1}, \boldsymbol{p}_{t-1}) = \max\{Q_t(\boldsymbol{\omega}_{t-1}, \boldsymbol{p}_{t-1}; \boldsymbol{\xi}_t) : \boldsymbol{\xi}_t \in \Xi_t\} \tag{28}$$

where $Q_t(\boldsymbol{\omega}_{t-1}, \boldsymbol{p}_{t-1}; \boldsymbol{\xi}_t)$ is defined as:

$$\begin{aligned} Q_t(\boldsymbol{\omega}_{t-1}, \boldsymbol{p}_{t-1}; \boldsymbol{\xi}_t) = \min\ & \boldsymbol{m}_t^{\top}\boldsymbol{p}_t + \mathcal{Q}_{t+1}(\boldsymbol{\omega}_t, \boldsymbol{p}_t) \\ s.t.\ & \boldsymbol{\omega}_t = \boldsymbol{\omega}_{t-1} \\ & \boldsymbol{D}_t\boldsymbol{p}_{t-1} + \boldsymbol{B}_t\boldsymbol{p}_t + \boldsymbol{E}_t\boldsymbol{\omega}_t\boldsymbol{e}_t \le \boldsymbol{F}_t\boldsymbol{\xi}_t \\ & \boldsymbol{p}_t \in \mathbb{R}^n,\ \boldsymbol{\omega}_t \in \mathbb{R}^{m\times T} \end{aligned} \tag{29}$$

In (27) and (29), the linking constraints $\boldsymbol{\omega}_1 = \boldsymbol{w}$ and $\boldsymbol{\omega}_t = \boldsymbol{\omega}_{t-1}$ copy the WAC assessment decision $\boldsymbol{w}$ obtained by solving Q_P to the state space of each stage problem. It means that not only the variable $\boldsymbol{p}_t$ representing system operation state (e.g. units ramping state), but $\boldsymbol{\omega}_t$ are state variables in the proposed WAC assessment model. This state space augmentation technique for the feasibility of the whole multi-stage RO problem is proved in our previous study [31].

4. Problem solving methodology

4.1. Two-bounds based optimal solution method

Due to the dynamic programming based framework, the problem (26)-(29) can be solved recursively via decomposition methods. For the multi-stage SO based dynamic formulation, the nested Benders cut and SDDP can be employed to achieve the global optimal solution, which constructs the lower bounds of cost-to-go functions $\underline{\mathcal{Q}}_{t+1}$ through cutting planes. But in the multi-stage RO problem studied in this paper, using only lower bounds of cost-to-go functions cannot handle the nested "max" operator indicating the worst-case uncertainties realization [28], as in (28).

Consistent with the conventional RDDP method [28], both the lower bounds of cost-to-go functions $\underline{\mathcal{Q}}_{t+1}$ and the upper bounds $\overline{\mathcal{Q}}_{t+1}$ are constructed in FRDDP, which has the relationship $\underline{\mathcal{Q}}_{t+1} \le \mathcal{Q}_{t+1} \le \overline{\mathcal{Q}}_{t+1}$ with the real cost-to-go functions $\mathcal{Q}_{t+1}$. In RDDP, the $\overline{\mathcal{Q}}_{t+1}$ and $\underline{\mathcal{Q}}_{t+1}$ are constructed by convex hull and hyperplanes respectively, as shown in Fig. 4. This two-bounds based solution method can effectively screen out the worst scenario involved in $\mathcal{Q}_{t+1}$ via the refinement of upper bounds, and achieve the global optimal solution of multi-stage RO. To approximate $\mathcal{Q}_{t+1}$,

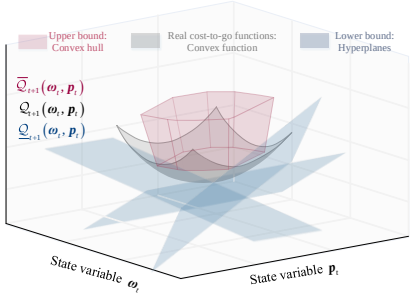

Fig. 4. Geometric interpretation of two-bounds based solution method in FRDDP

the $\underline{\mathcal{Q}}_{t+1}$ and $\overline{\mathcal{Q}}_{t+1}$ are refined iteratively until the gap between them is less than the criterion, which is completed by recursively solving the lower and upper approximation problems, $\underline{Q}_t$ and $\overline{Q}_t$.

$$\begin{aligned} \overline{Q}_t = \max_{\boldsymbol{\xi}_t\in\Xi_t} \min\ & \boldsymbol{m}_t^{\top}\boldsymbol{p}_t + \overline{\mathcal{Q}}_{t+1}(\boldsymbol{\omega}_t, \boldsymbol{p}_t) \\ s.t.\ & \begin{cases} \boldsymbol{\omega}_t = \boldsymbol{w}\ when\ t = 1 \\ \boldsymbol{\omega}_t = \boldsymbol{\omega}_{t-1}\ otherwise \end{cases} \\ & \boldsymbol{D}_t\boldsymbol{p}_{t-1} + \boldsymbol{B}_t\boldsymbol{p}_t + \boldsymbol{E}_t\boldsymbol{\omega}_t\boldsymbol{e}_t \le \boldsymbol{F}_t\boldsymbol{\xi}_t \\ & \boldsymbol{p}_t \in \mathbb{R}^n,\ \boldsymbol{\omega}_t \in \mathbb{R}^{m\times T} \end{aligned} \tag{30}$$

$$\begin{aligned} \underline{Q}_t(\boldsymbol{\xi}_t) = \min\ & \boldsymbol{m}_t^{\top}\boldsymbol{p}_t + \underline{\mathcal{Q}}_{t+1}(\boldsymbol{\omega}_t, \boldsymbol{p}_t) \\ s.t.\ & \begin{cases} \boldsymbol{\omega}_t = \boldsymbol{w}\ when\ t = 1 \\ \boldsymbol{\omega}_t = \boldsymbol{\omega}_{t-1}\ otherwise \end{cases} \\ & \boldsymbol{D}_t\boldsymbol{p}_{t-1} + \boldsymbol{B}_t\boldsymbol{p}_t + \boldsymbol{E}_t\boldsymbol{\omega}_t\boldsymbol{e}_t \le \boldsymbol{F}_t\boldsymbol{\xi}_t \\ & \boldsymbol{p}_t \in \mathbb{R}^n,\ \boldsymbol{\omega}_t \in \mathbb{R}^{m\times T} \end{aligned} \tag{31}$$

The implementation of FRDDP consists of two procedures: *Forward pass* and *Backward pass*. In the *Forward pass*, from pre-stage (Q_P) to stage T (Q_T), problem $\overline{Q}_t$ is solved to generate the worst-case uncertainty realization $\boldsymbol{\xi}_t$, and the decision sampling points $[\boldsymbol{\omega}_t; \boldsymbol{p}_t]$ are determined through the solution of problem $\underline{Q}_t(\boldsymbol{\xi}_t)$ under scenario $\boldsymbol{\xi}_t$. The *Backward pass* yields effective inner points, supporting hyperplanes to refine $\overline{\mathcal{Q}}_{t+1}$ and $\underline{\mathcal{Q}}_{t+1}$. The algorithm terminates once the upper bound reaches the lower bound.

Similar to the conventional RDDP, the lower bound $\underline{\mathcal{Q}}_{t+1}(\boldsymbol{\omega}_t, \boldsymbol{p}_t)$ contained in problem (31) is refined by adding Benders cutting planes in FRDDP. The cutting-plane based lower approximation problems at each stage remain feasible due to the presence of slack variables, and the optimal cuts (32) can be individually constructed without any feasible cuts to speed up computation [40].

$$\underline{\mathcal{Q}}_{t+1}(\boldsymbol{\omega}_t, \boldsymbol{p}_t) \geq \boldsymbol{\pi}_t^{\omega\top}(\boldsymbol{\omega}_t - \underline{\boldsymbol{\omega}}_t) + \boldsymbol{\pi}_t^{p\top}(\boldsymbol{p}_t - \underline{\boldsymbol{p}}_t) + \underline{Q}_{t+1}^* \tag{32}$$

where, $\underline{\boldsymbol{\omega}}_t$ and $\underline{\boldsymbol{p}}_t$ are the optimal solution of $\underline{Q}_t(\boldsymbol{\xi}_t)$ obtained from the just finished *Forward pass*. The $\underline{Q}_{t+1}^*$ is the value of objective function for the problem $\underline{Q}_{t+1}(\boldsymbol{\xi}_{t+1})$ in this round *Backward pass*, and $[\boldsymbol{\pi}_t^{\omega}; \boldsymbol{\pi}_t^{p}]$ represents the shadow price of $[\underline{\boldsymbol{\omega}}_t; \underline{\boldsymbol{p}}_t]$ in problem $\underline{Q}_{t+1}(\boldsymbol{\xi}_{t+1})$.

As for the formulation of upper bound $\overline{\mathcal{Q}}_{t+1}(\boldsymbol{\omega}_t, \boldsymbol{p}_t)$ in problem (30), the FRDDP proposed in our previous work [31] creates an approximated convex hull based methodology to avoid the huge computation in the upper approximation of conventional RDDP, which is detailed in section 4.2.

4.2. RIA based upper approximation

In the conventional RDDP, the convex hull based upper bound in Fig. 4 is formulated through the internal approximation (IA) method [28], which needs to enumerate the extreme points of $\overline{\mathcal{Q}}_{t+1}(\boldsymbol{\omega}_t, \boldsymbol{p}_t)$. This time consuming procedure in IA makes the conventional RDDP cannot solve the real-time dispatch problem even with more than ten units [29]. In the FRDDP algorithm, an RIA method is presented to accelerate the solution of upper approximation problem $\overline{Q}_t$, which avoids the extreme points enumeration via constructing an approximate convex hull. The RIA formulated problem $\overline{Q}_t$ in FRDDP is shown as following:

$$\begin{aligned}
\overline{Q}_t = \max_{\boldsymbol{\xi}_t \in \Xi_t} \min_{\lambda_s, \boldsymbol{\Delta}_t^+, \boldsymbol{\Delta}_t^-, \boldsymbol{\omega}_t, \boldsymbol{p}_t} \ & \boldsymbol{m}_t^\top \boldsymbol{p}_t + \overline{\mathcal{Q}}_{t+1}(\boldsymbol{\omega}_t, \boldsymbol{p}_t) \\
s.t.\ \ & \overline{\mathcal{Q}}_{t+1}(\boldsymbol{\omega}_t, \boldsymbol{p}_t) = \sum_{s \in \Lambda_t} \wp_s \lambda_s + \boldsymbol{l}_t^{\upsilon\top}(\boldsymbol{\Delta}_t^+ + \boldsymbol{\Delta}_t^-) \\
& \begin{cases} \boldsymbol{\omega}_t = \boldsymbol{w} \ \ when\ t = 1 \\ \boldsymbol{\omega}_t = \boldsymbol{\omega}_{t-1} \ \ otherwise \end{cases} \\
& \boldsymbol{D}_t \boldsymbol{p}_{t-1} + \boldsymbol{B}_t \boldsymbol{p}_t + \boldsymbol{E}_t \boldsymbol{\omega}_t \boldsymbol{e}_t \leq \boldsymbol{F}_t \boldsymbol{\xi}_t \\
& \sum_{s \in \Lambda_t} \lambda_s = 1,\ \lambda_s \geq 0,\ \forall s \in \Lambda_t \\
& \sum_{s \in \Lambda_t} \lambda_s [\boldsymbol{\omega}_t^s; \boldsymbol{p}_t^s] + \boldsymbol{\Delta}_t^+ - \boldsymbol{\Delta}_t^- = [\boldsymbol{\omega}_t; \boldsymbol{p}_t] \\
& \boldsymbol{\Delta}_t^+, \boldsymbol{\Delta}_t^- \geq 0,\ \boldsymbol{\Delta}_t^+ \in \mathbb{R}^{n+m\times T}, \boldsymbol{\Delta}_t^- \in \mathbb{R}^{n+m\times T} \\
& \boldsymbol{p}_t \in \mathbb{R}^n,\ \boldsymbol{\omega}_t \in \mathbb{R}^{m\times T}, \lambda_s \in \mathbb{R}^1
\end{aligned} \tag{33}$$

The illustration of (33) and its comparison with IA are shown geometrically in Fig. 5. As shown in Fig. 5(a), the IA method constructs the top of convex hull by enumerating all extreme points of $\overline{\mathcal{Q}}_{t+1}(\boldsymbol{\omega}_t, \boldsymbol{p}_t)$. After that, IA collects a decision sample point for each iteration in order to update the convex hull, which increasingly approaches the real cost-to-go function $\mathcal{Q}_{t+1}$ from above. In contrast, the RIA substitutes boundary lines with slope $\boldsymbol{l}_t^{\upsilon}$ for the extreme points-based top, to build up an approximate convex hull. If the optimal solution falls inside the approximate convex hull (shadow region in Fig. 5(b)), the $\overline{\mathcal{Q}}_{t+1}(\boldsymbol{\omega}_t, \boldsymbol{p}_t)$ is formulated as a convex combination of the historical inner points $\sum_{s \in \Lambda_t} \lambda_s [\boldsymbol{\omega}_t^s; \boldsymbol{p}_t^s]$. Whilst $\overline{\mathcal{Q}}_{t+1}(\boldsymbol{\omega}_t, \boldsymbol{p}_t)$ is penalized by a large number $\boldsymbol{l}_t^{\upsilon}\boldsymbol{\Delta}_t$ and locates on the boundary lines if the optimal solution lies outside of the approximate convex hull. Additionally, the validation, tightness and finite convergence of RIA method based FRDDP algorithm is mathematically proved in our prior work [31].

As for the solution of "max-min" problem (33), with the linearization of Big-M method, the duality theorem or Karush-Kuhn-Tucker optimality conditions can be used to transform it into a single layer MILP problem [12], which can be directly handled by commercial solvers.

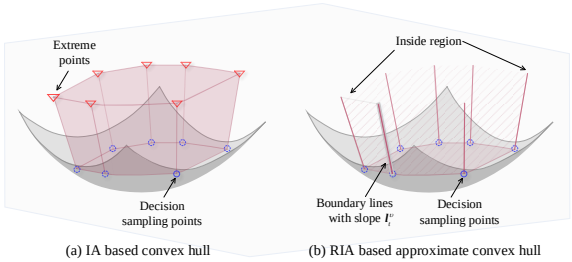

Fig. 5. Demonstration of the upper bounds of conventional RDDP and FRDDP

4.3. Adaptive accelerating technique

The FRDDP requires complete *Forward pass* and *Backward pass* from pre-stage to stage T, which constantly produces redundant cuts and inner points because $\underline{\mathcal{Q}}_{t+1}$ and $\overline{\mathcal{Q}}_{t+1}$ may converge earlier in some stages. Hence, we suggest an adaptive stage selection approach for the FRDDP, which is checked before each iteration.

$$T_{adp} = \text{findlast}\left(\left\{\frac{\overline{\mathcal{Q}}_t - \underline{\mathcal{Q}}_t}{\overline{\mathcal{Q}}_t} \geq \varepsilon,\ \forall t \in 1:T\right\}\right) \tag{34}$$

where, T_{adp} represents the end stage of the *Forward pass* and *Backward pass*. It is found by the last one whose relative gap of upper and lower bound is more than the tolerance ε.

Note that the effectiveness of adaptive stage selection is guaranteed by the fact that the cost-to-go functions in SDDP or RDDP always converge in the sequence from the T-stage problem to the first stage problem [28], [41]. Besides, when the gap between $\underline{\mathcal{Q}}_1$ and $\overline{\mathcal{Q}}_1$ is lower than the tolerance, the whole algorithm satisfies the convergence criterion.

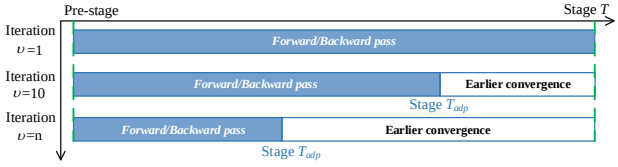

Fig. 6. Illustration of adaptive stage selection in FRDDP

In (33), the slope of approximated convex hull's boundary lines, $\boldsymbol{l}_t^{\upsilon}$, is a tuning parameter that has strong influence on the convergence of FRDDP. A too large value will result in an inside region that is too tiny to explore sufficient decision sampling points, which slows convergence. By contrast, a value that is too small could cause the lower bound to exceed the upper bound. For the feasibility of two-bounds based optimal solution method, the key observation is that the boundary slope of the outside region of $\overline{\mathcal{Q}}_{t+1}$ should be no less than the maximum slope of $\underline{\mathcal{Q}}_{t+1}$. Therefore, we present an adaptive rule to configure $\boldsymbol{l}_t^{\upsilon}$.

$$\boldsymbol{l}_t^{\upsilon} = \rho \cdot \max\left\{[\boldsymbol{\pi}_t^{\omega(k)}; \boldsymbol{\pi}_t^{p(k)}],\ \forall k \in 1:\upsilon(\upsilon \geq 2)\right\} \tag{35}$$

where, $[\boldsymbol{\pi}_t^{\omega(k)}; \boldsymbol{\pi}_t^{p(k)}]$ is the historical value of $[\boldsymbol{\pi}_t^{\omega}; \boldsymbol{\pi}_t^{p}]$ in iteration from 1 to υ. ρ is tested to be configured between 1.5 and 2.0, which will be more suitable to ensure that RIA is strictly above the real value function $\mathcal{Q}_{t+1}$. With the adaptive variability of $\boldsymbol{l}_t^{\upsilon}$, the approximate convex hull can explore

more decision sampling points at the start of FRDDP to speed up convergence, and ensure the strict optimality of the solutions at the end of the algorithm. In summary, the solution procedure of FRDDP is summarized in Fig. 7.

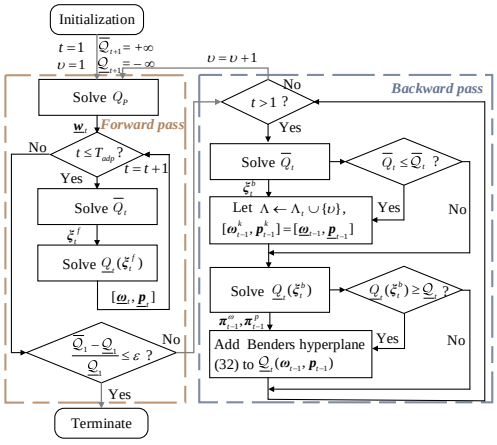

Fig. 7. Flow chart of FRDDP with adaptive acceleration

5. Case study

5.1. Simulation setting

The proposed method is tested on a modified IEEE 14-Bus (MI14B) system and a real-world system connecting Jiashan region, Pinghu region and Nanhu region in Zhejiang province of China, the topology of which are drawn in Fig. 8 and Fig. 9. The MI14B system consists of 3 dispatchable units, 2 ESS, 1 wind farm and 1 fast-starting emergency generator (FEG). The interconnected three regions of the real-world system have 39, 18 and 44 buses, respectively, whose tie lines are marked by red. The number of transmission lines, generation units, and wind farms involved in the three regions are shown by Table 2. Ref. [42] aggregates the day-ahead forecast information of demand and wind generation, detailed parameters of each equipment and capacities of transmission lines. The penalty coefficient of power imbalance M is set as 10^6 \$/MWh, and the risk coefficients of WCR and LSR, c_q^u and c_q^d, are configured by 50 \$/MWh and 10^4 \$/MWh. The minimum on/off time of fast-starting units is 1 hour, whose start-up and fuel cost are 4×10^3 \$ and 10^3 \$/MWh. Each wind farm's actual available power is assumed to follow a normal distribution, whose standard deviation σ equals 0.1 $AW_{q,t}$. The test code is implemented on JuMP.jl toolkit of the Julia language, and the optimization problems are solved by Gurobi Optimizer 8.1.1 on a server with CPU Xeon E5–2678, 64 Gb RAM. Four cases are designed to demonstrate the effectiveness of the proposed methodologies, where three other WAC assessment methods are introduced for comparison.

Table 2. Characteristics of real-world test system

District	Jiashan Region	Pinghu Region	Nanhu Region
Buses	39	18	44
Dispatchable Units	7	4	7
ESS	4	2	3
Transmission Line	46	26	52
FEG	3	2	3

Case I: Static WAC assessment based on the two-stage RO [34], which does not consider the system operational risk.

Case II: Risk based WAC assessment formulated by the two-stage RO [5], [6], which ignores the non-anticipativity of decision making under the uncertain wind evolution.

Case III: Extending Case II into a non-anticipative multi-stage RO scheme, which uses affine rules [22], [23] to obtain the approximate optimal solution. It's worth noting that although most affine rules applied to power system problems map the recourse decisions to a linear function of the current uncertainty realization [43] or the current forecast error [44], it has been demonstrated that the affine rule mapping historical uncertainty information, termed the full affine rule, can achieve superior solution quality in addressing multi-stage RO problems, as detailed in [16], [22], and utilized in [23]. Given the focus of this study on day-ahead WAC assessment, there is ample time for the model solution to be conducted. Consequently, we adopt the more precise full affine rules for comparison in this section. For a more comprehensive comparison between the FRDDP, current information-based affine rules, and full affine rules concerning the solution of multi-stage RO in terms of computational tractability and solution quality across both day-ahead and intra-day timescales, we refer readers to our previous work [31].

Case IV: The proposed WAC assessment method, which uses FRDDP algorithm to obtain the global optimal solution.

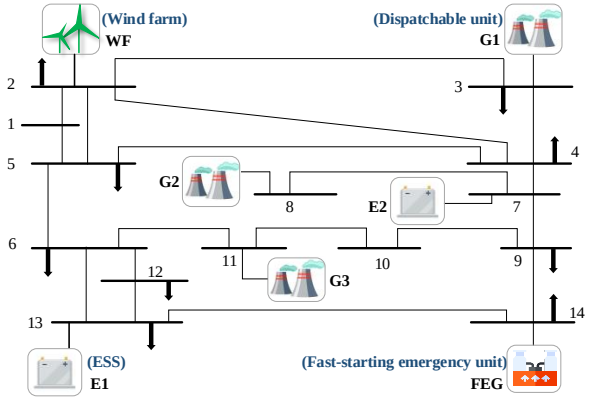

Fig. 8. Topology of the modified IEEE 14-Bus system

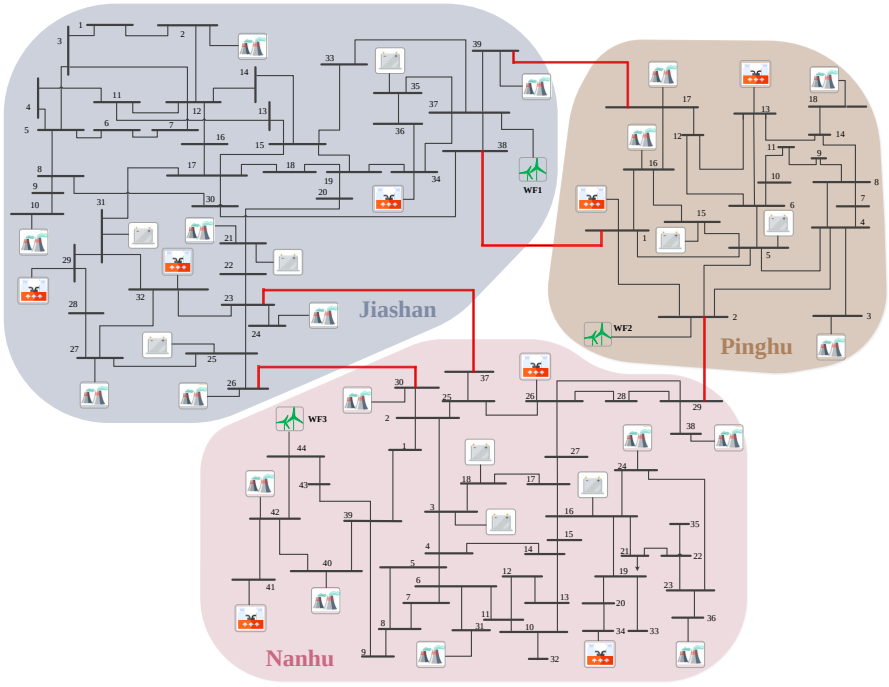

Fig. 9. Topology of the three-region connected real-world system in Zhejiang province, China

In each case, the WAC assessment is conducted based on the day-ahead forecast information and pre-given UC. To make the best usage of the clean energy, we stipulate the operators will purchase the upper amount of WAC range if the actual available wind energy on the real-time power market exceeds the maximum admissible level. While the fast-starting units will be used to meet the load if the actual wind energy available cannot reach the lower admissible bound. The specific real-time ED model considering the participation of FEG in each case for validating the WAC assessment results can be found in [45].

5.2. The results of the Modified IEEE 14-Bus system

The day-ahead pre-defined UC of MI14B system is drawn by Fig. 10. For Cases I-IV, the WAC assessment results of the MI14B system are compared in Fig. 11, where the day-ahead forecast wind generation data with different confidence interval are also demonstrated. In Fig. 11, Case I determines a static WAC range that exactly consists of the boundary of two-stage RO's box uncertainty sets. Compared with Case I, considering the operational risk, Case II obtains a WAC assessment result which has larger admissible capacity and more flexible boundaries. For Case III and IV, the flexibility of admissible boundary is preserved while the WAC range is smaller than that in Case II. The reason is that the two-stage RO method used in Case II ignores the non-anticipativity of assessment decisions, which overestimates the adjustable capability of dispatchable elements to accommodate variable wind power. Besides, Case IV behaves with larger WAC range than Case III, since the affine approximation used in Case III loses the optimality of solutions. To further evaluate the quantity of WAC of Cases II-IV, the calculated operational risk values and other solution information are provided in Table 3.

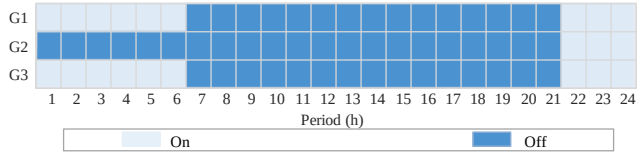

Fig. 10. Pre-given UC information of the MI14B system

Table 3. Risk comparison of Cases I-IV on the MI14B system

Case	Operational risk ($)	Imbalanced Power (MW)	Running time (sec.)
I	\	0.0026	67.05
II	419.91	0.0053	69.33
III	986.35	0.0097	264.15
IV	530.77	0.0049	80.96

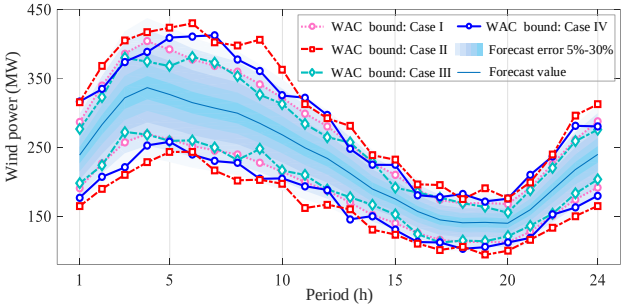

Fig. 11. Determined WAC assessment results of Cases I-IV

The imbalanced power in each case is less than 10^{-2} MW in Table 3, which means the security constraints will be satisfied within the WAC range. Among all the cases, the operational risk of Case II is lowest in Table 3, which denotes the allowable WAC interval is the widest, in accordance with Fig. 11. Although Case III extends the two-stage scheme into multi-stage to enforce assessment decisions' non-anticipativity, the historical affine information aggravates the computational burden, and lengthens the computation time. To validate the effectiveness of the WAC assessments of Cases I-IV for intra-day wind energy trading, 10,000 possible wind generation scenarios with forecast error 20% are sampled by the Monte Carlo method (MC) [12] to simulate the real-time measured wind power data. The MC outcomes of each case for intra-day dispatch considering real-time wind power trading is provided in Table 4.

Table 4. Statistic outcomes of Cases I-IV in MC testing on MI14B system

Case	Wind curtailment ($)	Load shedding ($)	Generation cost of FEG ($)	Total cost ($)
I	8,518.56	5,360.32	30,721.46	123,601.79
II	11,844.96	3,414.92	21,964.42	85,377.04
III	9,502.23	2,609.91	28,907.61	106,349.90
IV	6,019.13	1,878.36	22,139.55	61,511.21

Table 5. Total cost of Cases I-IV under different forecast errors in MC

Case	Total cost ($) / under MC's forecast error percentage:			
	5%	10%	20%	30%
I	89,675.08	98,872.00	123,601.79	152,057.96
II	63,782.61	74,276.18	85,377.04	101,343.85
III	80,134.90	88,475.30	106,349.90	131,702.83
IV	46,976.30	53,536.22	61,511.21	82,219.64

According to Table 4, although the majority of the bought wind energy in Case I can be used within a narrow WAC range, there will be a significant increase in the generation costs for FEG and other dispatchable units due to the insufficient wind generation. Between Cases III and IV, Case IV's assessment decision can better handle the actual intra-day dispatch process because it naturally characterizes the dynamic operation of generators and ESS via the global optimal framework. For Case II and Case IV, Case IV performs better in wind curtailment and in making economic generation decisions since it takes into account the non-anticipativity of the uncertain evolution of wind power, which will be demonstrated in more detail later. Compared with existing studies, the proposed assessment method reduces the wind curtailment by 29.34%.

Furthermore, different forecast errors of wind power are configured in MC sampling to compare the performances of Cases I-IV to check the results above. The total operation cost of Cases I-IV under MC forecast error 5%-30% is provided Table 5. It is found in Table 5 that the total operation cost increases along with the growth of forecast error in each case, while the ranks analyzed in Table 4 remain unchanged. Compared with the best-performed assessment method among the existing researches, Case III, the Case IV reduces the total operational cost by at least 18.87%.

To demonstrate the impact of considering / not considering the non-anticipativity of uncertain wind evolution on the effectiveness of WAC assessment, a typical available wind generation scenario (dotted line) involved in MC sampling is screened out to compare the decisions made in Case II and Case IV, which is drawn in Fig. 12.

The WAC assessment outcomes and corresponding intra-day elements' generation decision of Cases II and IV are shown in Fig. 12(a) and Fig. 12(b), respectively. When the available wind power is at a high level, such as periods 5-9h and 13-18h, Case IV only purchases the upper bound of admissible interval since the admissible range cannot envelope the total wind generation. Case II, on the other hand, buys all of the available wind energy because it overestimates the generators' adjustable capacity to get a broader WAC range that can include all of the available wind energy, which leads to a significant wind curtailment. In Case IV, the MEG units are started up to meet the load during periods of low wind power availability, such as 10-12h and 22-24h, because the actual wind power is less than the WAC limitation. However, Case II incorrectly assumes that since the wind output is within the WAC range, the load would be provided by dispatchable elements, resulting in load shedding.

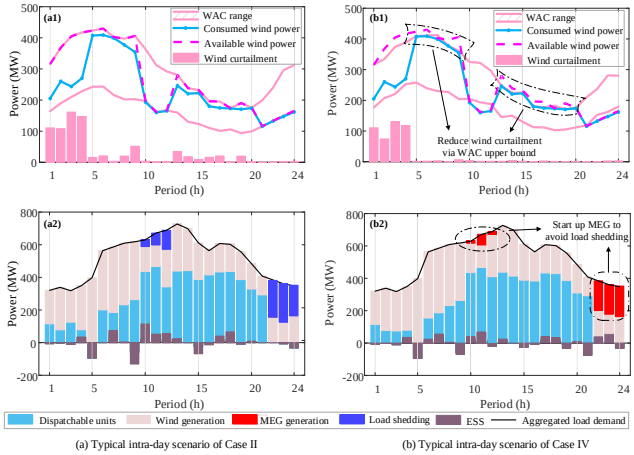

Fig. 12. Comparison of the decisions considering / not considering non-anticipativity

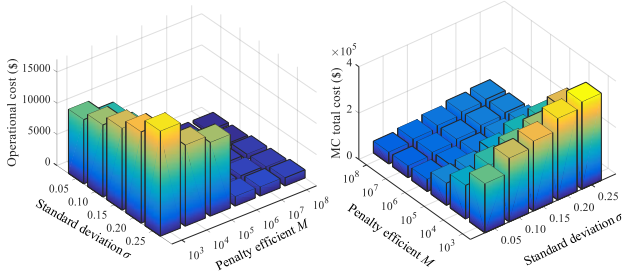

Fig. 13. Impacts of important parameters on the WAC assessment results

Moreover, the influences of penalty coefficient M for imbalanced power and the standard deviation σ are studied, which is shown in Fig. 13. It can be seen that the operational risk and MC total cost, which is the sum of the wind curtailment cost, load shedding cost and total fuel cost, increase along with the growth of the standard deviation σ. Besides, the assessment can degenerate into a deterministic optimization problem with operational risk equal to zero if there is no forecast error. With the increment of M, the system's operational risk and MC total cost initially rise and then nearly stays the same, indicating that the worst-case scenario filtered out by the multi-stage RO will not change when M is larger than 10^6.

5.3. The results of the three-region connected real-world system

In the real-world system, a 31-days real wind power and load data from 00:00 August 1, 2021 to 23:45 August 31, 2021 in [46] is employed as the basic value of forecast and real measured wind power to perform the proposed assessment methodology. The total installed capacity of wind generation is set by 36% of the installed thermal generation, where the proportion of wind farm (WF) 1-3 are configured by 33.60%, 23.92%, 42.48%, respectively. The original load data is expanded by the same ratio with wind generation capacity and averagely distributed to each bus.

The WAC admissible output of the real-world system with the 31-days simulation is shown by Fig. 14. It can be seen from Fig. 14 (a) that the real wind power locates in the WAC range in most periods. If the real wind generation cannot achieve the admissible lower bound, the load beyond the capacity of the EMG unit will be shed, as shown in Fig. 14 (b). As highlighted in Fig. 14(c), surplus wind power may be curtailed when the real wind power exceeds the WAC range. Overall, the obtained WAC range effectively directs the cooperation between intra-day dispatch and real-time trading of wind energy, since the wind curtailment and load shedding are less than 9.35% and 4.22% in Fig. 14(d), respectively.

Table 6. Daily average outcomes of Cases I-IV with 31-days simulation

Case	Running time (sec.)	Operational risk ($)	Operation total cost ($10^3$$)
I	313.34	\	1,015.41
II	328.98	7,190.18	701.47
III	1,092.77	13,874.16	882.60
IV	299.62	8,560.23	553.39

To verify the effectiveness of proposed assessment method, Cases I-IV are tested on the real-world system using the 31-days real wind data, whose daily average outcomes are displayed in Table 6. Table 6 has similar results with Table 3 and Table 4, indicating that Case IV provides a more practical assessment scheme for WAC, which can guide the operators make more economical decisions in real-world intra-day dispatch and wind power trading. In contrast to Table 3, Case IV in Table 6 takes less time than Cases I and II in real-world system. The rationale is that each stage problem in Case IV is decoupled from the others, and that as a result of the exponentially decreasing dimensionality of the optimization variables for large-scale systems, the computation complexity of the LP problem has been considerably reduced.

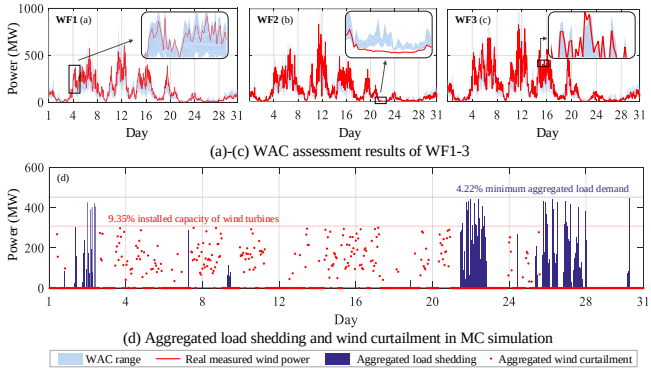

Fig. 14. WAC assessment outcomes and analyses of the real-world system

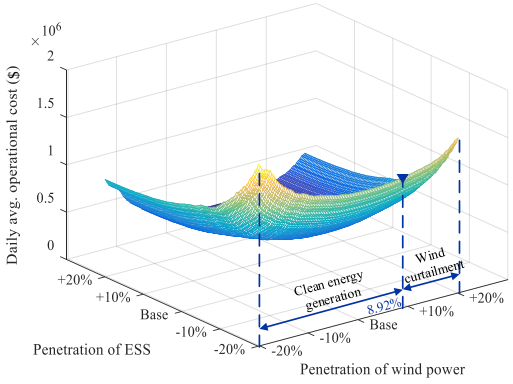

Fig. 15. Performance of WAC-range guided intra-day dispatch under different wind power and ESS penetration levels

Furthermore, we compare the WAC-range guided intra-day dispatch and real-time trading under different wind energy and ESS penetration levels in the real-world system. The resolution for varying the capacities of ESS and wind generation is assumed as 0.5% in Fig. 15. Since the ESS is crucial for peak clipping and valley filling for power systems, which mitigates the impact of wind power variations on the precision of WAC intervals, the operational cost reduces as ESS capacity increases. While the operation cost initially decreases and then reversely increases as installed wind production capacity increases, this is because a suitable increase can reduce the cost of thermal units, but a massive increase will result in a significant rise in the WCR risk for the system.

5.4. Performance of FRDDP algorithm with adaptive acceleration

The finite convergence of FRDDP has been mathematically proved in our previous work [31]. To trace the development of upper bound and lower bound in the iteration of FRDDP algorithm, the solution procedures for the WAC assessment model on the MI14B system and the real-world system are depicted in Figs. 16(a) and 16(b), respectively. Additionally, Fig. 16(c)-(d) show how the presented adaptive stage reduction evolved.

Fig. 16(a)-(b) show after the opposite evolution of upper and lower bound, the FRDDP can tightly converge to the optimality gap of 0.1% on different test systems. To verify the stability of the FRDDP algorithm, the two iteration processes were tested 100 times, which comes out that the results remain the same. This is because the FRDDP is a deterministic algorithm, where the sampling points are obtained and boundaries are adjusted in an orderly manner, which is different from similar stochastic algorithms like SDDP. This characteristic makes FRDDP is beneficial for the application to industry. In Fig. 16(c)-(d), the adaptive acceleration technique is checked at the end of each iteration in FRDDP to screen out the earlier converged stage problems, which effectively reduces the number of stages that needs to be solved in the *Forward* and *backward pass* procedure. During the final iteration process of MI14B and real-world systems, the problems to be solved in FRDDP were reduced to from pre-stage to stage 5, and to stage 7, respectively.

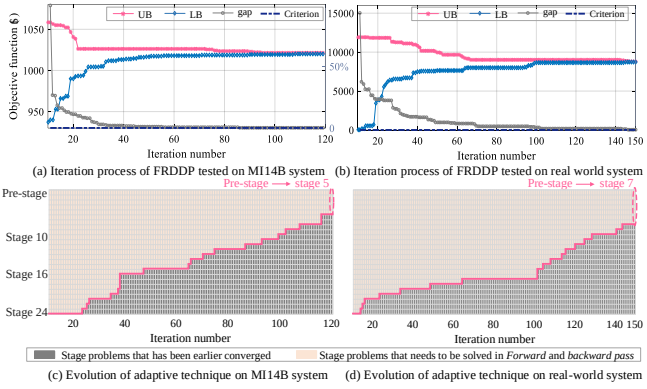

Fig. 16. Evolution of FRDDP iteration with adaptive technique

Table 7. Comparison of FRDDP with and without adaptive acceleration

Items	MI14B		Real-world system	
	Adaptive acceleration	Without acceleration	Adaptive acceleration	Without acceleration
Final upper bound (10^3 $)	1.0212	1.0212	8.7604	8.7604
Final lower bound (10^3 $)	1.0201	1.0201	8.7527	8.7527
Total iteration number	120	120	150	150
Minimum computation time/ iteration (sec.)	0.3351	1.9411	0.9987	4.2052
Total time consumption (sec.)	142.9640	376.5823	299.6216	1,124.1921

To study the effectiveness of presented adaptive acceleration technique for FRDDP algorithm, the performance of FRDDP algorithm with and

without integrating acceleration technique is demonstrated in Table 7. According to Table 7, the FRDDP converges with the same number of iterations no matter whether the acceleration techniques is adopted, with the upper and lower bounds having the same value at the end of each iteration. Nevertheless, each iteration's computational speed of FRDDP with acceleration technique has significantly improved, which is particularly noticeable in large-scale systems. The reason is that the acceleration technologies effectively decrease the number of unsolved problems and offer more flexible boundaries. Compared to the original FRDDP algorithm, the proposed adaptive acceleration technique reduces the computational consumption by 62.04% and 73.34% on MI14B system and real-world system, respectively.

6. Conclusion

In this paper, a robust and non-anticipative method is proposed for conducting quantitative WAC assessment for wind power penetrated power systems, which can offer useful recommendations for the wind energy trading in real-time power market. The presented assessment model is formulated via a multi-stage RO problem, which addresses the anticipativity issues in the traditional two-stage method while maintaining the decision-making process' robustness. The multi-stage RO model successfully incorporates a tractable risk assessment mechanism to create dynamic admissible boundaries for the WAC range. Additionally, a novel FRDDP algorithm is employed to achieve global optimal solutions of the assessment model, which integrates adaptive strategies to accelerate convergence.

Numerical results are presented to validate the effectiveness of the proposed WAC assessment method and adaptive acceleration technique. Key findings are drawn as follows: 1) According to the MC simulation conducted on the MI14B system, the proposed risk-based assessment method, in comparison to existing studies, effects a reduction of 18.87% in total operational cost and diminishes wind curtailment by 29.34% when guiding the real-time wind power trading and dispatch. 2) With non-anticipative admissible WAC boundaries, the proposed method can activate the MEG units promptly to meet the load requirement under extreme conditions, which effectively avoids load shedding. 3) The presented adaptive acceleration technique significantly improves the computational speed of FRDDP, which is particularly noticeable in large-scale systems. When applied to resolve the WAC assessment for real-world systems, it reduces the computational consumption by 73.34% for original FRDDP algorithm. These factors suggest that this work could develop into a promising alternative strategy for the WAC assessment of real-world wind energy penetrated power systems, which opens up avenues for future research.

References

[1] Zhou Y, Manea A, Hua W, Wu J, Zhou W, et al. Application of distributed ledger technology in distribution networks. Proc of the IEEE 2022;110(12):1963-1975.

[2] Jing R, Hua W, Lin J, Lin J, Zhao Y, Zhou Y, Wu J. Cost-efficient decarbonization of local energy systems by whole-system based design optimization. Appl Energy 2022;326:119921.

[3] Yan M, Gan W, Zhou Y, Wen J, Yao W. Projection method for blockchain-enabled non-iterative decentralized management in integrated natural gas-electric systems and its application in digital twin modelling. Appl Energy 2022;311:118645.

[4] Zhou Y, Wu J, Song G, Long C. Framework design and optimal bidding strategy for ancillary service provision from a peer-to-peer energy trading community. Appl Energy 2020;278(15):115671.

[5] Wang C, Liu F, Wang J, Wei W, Mei S. Risk-based admissibility assessment of wind generation integrated into a bulk power system. IEEE Trans Sustain Energy 2016;7(1):325-336.

[6] Tan H, Ren Z, Yan W, Wang Q, Mohamed M. A. Wind Power Accommodation Capability Assessment Method for Multi-Energy Microgrids. IEEE Trans Sustain Energy 2021;12(4):2482-92.

[7] Du E, Zhang N, Hodge B, Wang Q, Lu Z, Kang C, et al. Operation of a high renewable penetrated power system with CSP plants: a look-ahead stochastic unit commitment model. IEEE Trans Power Syst 2019;34(1):140–51.

[8] Li K, Yang F, Wang L, Yan Y, Wang H, Zhang C. A scenario-based two-stage stochastic optimization approach for multi-energy microgrids. Appl Energy 2022;322:119388.

[9] Al-Lawati R, Crespo-Vazquez J, Faiz T, Fang X, Noor-E-Alam M. Two-stage stochastic optimization frameworks to aid in decision-making under uncertainty for variable resource generators participating in a sequential energy market. Appl Energy 2021;292:116882.

[10] Rostampour V, Haar O, Keviczky T. Distributed Stochastic Reserve Scheduling in AC Power Systems With Uncertain Generation. IEEE Trans Power Syst 2019;34(2):1005-20.

[11] Yanikoglu I, Gorissen B, den Hertog D. A survey of adjustable robust optimization, Eur J Oper Res 2019;277(3):799-813.

[12] Chen Z, Li Z, Guo C, Wang J, Ding Y. Fully Distributed Robust Reserve Scheduling for Coupled Transmission and Distribution Systems, IEEE Trans Power Syst 2021;36(1):169-82.

[13] Yan M, Zhang N, Ai X, Shahidehpour M, Kang C, Wen J. Robust two-stage regional-district scheduling of multi-carrier energy systems with a large penetration of wind power. IEEE Trans Sustain Energy 2019;10(3):1227–39.

[14] Fan W, Ju L, Tan Z, Li X, Zhang A, et al. Two-stage distributionally robust optimization model of integrated energy system group considering energy sharing and carbon transfer. Appl Energy 2023;331:120426.

[15] Wu M, Xu J, Zeng L, Li C, Liu Y, et al. Two-stage robust optimization model for park integrated energy system based on dynamic programming. Appl Energy 2022;308:118249.

[16] Lorca A, Sun X, Litvinov E, Zheng T. Multistage adaptive robust optimization for the unit commitment problem. Oper Res 2016;64(1):32–51.

[17] Helseth A, Fodstad M, Mo B. Optimal Hydropower Maintenance Scheduling in Liberalized Markets, IEEE Trans Power Syst 2018;33(6):6989-998.

[18] Aaslid P, Korpas M, Belsnes MM, Fosso O. Stochastic Optimization of Microgrid Operation With Renewable Generation and Energy Storages, IEEE Trans Sustain Energy 2022;13(3):1481–91.

[19] Xiong H, Yan M, Guo C, Ding Y, Zhou Y. DP based multi-stage ARO for coordinated scheduling of CSP and wind energy with tractable storage scheme: Tight formulation and solution technique. Appl Energy 2023;333:120578.

[20] Papavasiliou A, Mou Y, Cambier L, Scieur D. Application of Stochastic Dual Dynamic Programming to the Real-Time Dispatch of Storage Under Renewable Supply Uncertainty. IEEE Trans Sustain Energy 2018;9(2):547-58.

[21] Costa L, Thomé F, Garcia J, Pereira M. Reliability- Constrained Power System Expansion Planning: A Stochastic Risk-Averse Optimization Approach. IEEE Trans Power Syst 2021;36(1):97-106.

[22] Lorca A, Sun X. Multistage robust unit commitment with dynamic uncertainty sets and energy storage, IEEE Trans Power Syst 2017;32(3):1678-88.

[23] Abdin A, Caunhye A, Zio E, Cardin M. Optimizing generation expansion planning with operational uncertainty: a multistage adaptive robust approach. Appl Energy 2022;306:118032.

[24] Qiu H, Wang L, Gu W, Pan G, Ning C, Wu Z, Sun Q. Multistage scheduling of regional power grids against sequential outage and power uncertainties. IEEE Trans on Smart Grid 2022;13(6):4624-37.

[25] Ben-Tal A, Housni O, Goyal V. A tractable approach for designing piecewise affine policies in two-stage adjustable robust optimization. Math Program 2018;182(1): 57–102.

[26] Ardestani-Jaafari A, Delage E. Robust optimization of sums of piecewise linear functions with application to inventory problems. Oper Res 2016;64(2):474–94.

[27] Bertsimas D, Lancu D, Parrilo P. A hierarchy of near-optimal policies for multistage adaptive optimization. IEEE Trans Automat Contr 2011;56(12):2803–18.

[28] Georghiou A, Tsoukalas A, Wiesemann W. Robust dual dynamic programming. Oper Res 2019;67(3):813–30.
[29] Shi Y, Dong S, Guo C, Chen Z, Wang L. Enhancing the flexibility of storage integrated power system by multi-stage robust dispatch. IEEE Trans Power Syst 2022;36(3):2314–22.
[30] Qiu H, Sun Q, Lu X, Gooi HB, Zhang S. Optimality-feasibility-aware multistage unit commitment considering nonanticipative realization of uncertainty. Appl Energy 2022;327:120062.
[31] Xiong H, Shi Y, Chen Z, Guo C, Ding Y. Multi-stage robust dynamic unit commitment based on pre-extended -fast robust dual dynamic programming. IEEE Trans Power Syst 2023;38(3):2411-22.
[32] Yıldıran U. Robust multi-stage economic dispatch with renewable generation and storage. Eur J Oper Res 2023;309(2):890-909.
[33] Guo Y, Han X, Zhou X, Hug G. Incorporate day-ahead robustness and real-time incentives for electricity market design. Appl Energy 2023;332:120484.
[34] Zhao J, Zheng T, Litvinov E. Variable resource dispatch through do-not-exceed limit. IEEE Trans Power Syst 2015;30(2):820-28.
[35] Wang C, Gong Z, Liang Y, Wei W, Bi T. Data-Driven Wind Generation Admissibility Assessment of Integrated Electric-Heat Systems: A Dynamic Convex Hull-Based Approach. IEEE Trans Smart Grid 2020;11(5):4531-43.
[36] Wang C, Wang S, Liu F, Bi T, Wang T. Risk-Loss Coordinated Admissibility Assessment of Wind Generation for Integrated Electric-Gas Systems. IEEE Trans Smart Grid 2020;11(5), 4454-65.
[37] Liu J, Long Q, Liu, Liu R, Liu Wen, Hou Y. Online distributed optimization for spatio-temporally constrained real-time peer-to-peer energy trading. Appl Energy 2023;331:120216.
[38] Hakimi S, Hasankhani A, Shafie-khah M, Catalao J. Stochastic planning of a multi-microgrid considering integration of renewable energy resources and real-time electricity market. Appl Energy 2021;298:117215.
[39] Zhang N, Kang C, Xia Q, Ding Y, Huang Y, et al. A convex model of risk-based unit commitment for day-ahead market clearing considering wind power uncertainty. IEEE Trans Power Syst 2015;30(3):1582-92.
[40] Xiong H, Chen Z, Zhang X, Wang C, Shi Y, Guo C. Robust Scheduling with Temporal Decomposition of Integrated Electrical-Heating System Based on Dynamic Programming Formulation. IEEE Trans Ind Appl 2023, early access. doi: 10.1109/TIA.2023.3263385
[41] Regan B, Downward A, Zakeri G. A deterministic algorithm for solving multistage stochastic programming problems. Optim Online 2017;1-25.
[42] Data of MI14B and Three region connected real-world system [Online]. Available: https://drive.google.com/file/d/11vmhLaF5IWaSBDqKSJ6i-h0jI0IhHTYH/view?usp=share_link
[43] Li J, Khodayar M, Wang J, Zhou B. Data-Driven Distributionally Robust Co-Optimization of P2P Energy Trading and Network Operation for Interconnected Microgrids. IEEE Trans Smart Grid 2021; 12(6):5172-84.
[44] Li P, Yu D, Yang M, Wang J. Flexible Look-Ahead Dispatch Realized by Robust Optimization Considering CVaR of Wind Power. IEEE Trans Power Syst 2018;33(5):5330-40.
[45] Cobos N, Arroyo J, Alguacil N, Street A. Robust Energy and Reserve Scheduling Under Wind Uncertainty Considering Fast-Acting Generators. IEEE Trans Sustain Energy 2019;10(4):2142-51.
[46] Real wind power and load data from Eirgrid [Online]. Available: https://www.eirgridgroup.com/how-the-grid-works/system-information/

Acknowledgment

This work is supported by the supported by the State Key Program of National Natural Science Foundation of China (U22B2098), the National Natural Science Foundation of China (51537010), and in part by a USYD-ZJU Partnership Collaboration Award.